Int. J. Electrochem. Sci., 11 **(2016)** 1282 - 1292

International Journal of
ELECTROCHEMICAL
SCIENCE
www.electrochemsci.org

$(La_{1.66}Mg_{0.34})Ni_7$-based alloys : Structural and Hydrogen Storage Properties

Zhijie Gao [*], *Huiming Zhang*

Department of Chemistry and Chemical Engineering, Binzhou University, Binzhou 256600, PR China
[*]E-mail: gaozhijie1983@126.com

Received: 6 November 2015 / *Accepted:* 25 November 2015 / *Published:* 1 January 2016

The structural and hydrogen storage properties of $(La_{1.66}Mg_{0.34})Ni_7$-based alloys (i.e., A_2B_7-type) with a main structure (hexagonal Ce_2Ni_7-type) are investigated in this study. In Ce_2Ni_7-type structure, upon hydrogen the approximately single phase sample of the intermetallic compound with $(La_{1.66}Mg_{0.34})Ni_7$ expands isotropically, in contrast to the Mg free phase and $La_{0.63}R_{0.2}Mg_{0.17}Ni_{3.1}Co_{0.3}Al_{0.1}$ alloy. A decrease in the A-atomic radius and an increase in the B-atomic radius stabilize the metal sublattice and increase the reversible hydrogen storage capacity. The unit cell parameters in $La_{0.63}R_{0.2}Mg_{0.17}Ni_{3.1}Co_{0.3}Al_{0.1}$ alloy is almost no change during hydrogenation and the amorphous effect is very slight, compared to pure La_2Ni_7, which easily become amorphous upon hydrogen absorption-desorption cycling.

Keywords: Rare earth elements, Alloy structure, Unit cell volume, Equilibrium pressure, Electrochemical properties

1. INTRODUCTION

Hydrogen storage alloys have been attached more and more importance to application with “Hydrogen Energy” and research with “Ni/MH battery” put forward [1-3]. Rare-earth-based AB_5-type alloy and Zr-based Laves phase alloy have been commercialized successfully as Ni/MH secondary cell negative materials [4,5], but low capacity of AB_5-type alloy electrodes and difficult activation characteristics of Laves phase alloy electrodes limit the extensive application [6,7]. Many electrode materials are regarded as promising energy storage applications due to their powerful and reversible electrochemical redox reactions [8].

Since the use of $LaMg_2Ni_9$, La_2MgNi_9 and $La_5Mg_2Ni_{23}$ compounds was reported as hydrogen storage materials [9-11], ternary R-Mg-Ni (R = rare earth metals) compounds have been studied because their hydrogen storage properties are superior to corresponding binary AB_n (n = 2-5) compounds [12-25]. High hydrogen capacity, moderate hydrogen equilibrium pressure as well as light and less expensive elements makes them remarkable from an economical point of view. On the other hand, unknown structural properties raise the need for basic, crystallographic research. Recently, details about the structures of $Ce_2Ni_7H_{4/4.7}$ [26, 27], $Ce_2MgCo_9H_{12}$ [28], $La_2Ni_7H_{6.5}$ [29], $La_2Ni_7H_x$ (x = 6.4, 10.8) [13], $La_{1.5}Mg_{0.5}Ni_7H_{9.3}$ [30], $La_{1.63}Mg_{0.37}Ni_7D_{8.8}$ [31] and $La_4MgNi_{19}H(D)_x$ [16, 18, 19, 21] have been published, but little is known about the (R, Mg)$_2$Ni$_7$-H system. The effect of R substitution on the structural properties and electrochemical hydrogenation behavior of $La_{0.63}R_{0.2}Mg_{0.17}Ni_{3.1}Co_{0.3}Al_{0.1}$ have been investigated recently [32]. However, this data left open questions concerning the structures of the corresponding hydrides and influence of the R substitution on the structural and hydrogen gas sorption characteristics in such compounds. Furthermore, previous research revealed that the crystal structure of a binary R_2Ni_7 compound is size dependent; viz., the Ce_2Ni_7-type structure is stable for larger R-atomic radii, the Gd_2Co_7-type structure is preferred for smaller M-atomic radii, and both structures coexist in the case of medium-sized R-atomic radii [33]. This phenomenon also raises the question as to whether the crystal structure of ternary (R, Mg)$_2$Ni$_7$ compounds is also size dependent similar to binary R_2Ni_7 compounds. To clarify these two questions, the structure stabilities of Ce_2Ni_7- or Gd_2Co_7-type were studied by comparing their relative amounts in the $(La_{1.66}Mg_{0.34})Ni_7$-based compounds after partial substitution by different elements. On the basis of the $(La_{1.66}Mg_{0.34})Ni_7$ compound, Ce, Pr, Nd, Y, Sm and Gd are used as smaller substitutes for La, respectively, to change the average A-atomic radius. Similarly, Ni is partially replaced by Co and Al to increase the average B-atomic radius because Ni has the smallest atomic radius among transition metals.

From a hydrogen storage point of view, $(La_{1.5}Mg_{0.5})Ni_7$ with a Ce_2Ni_7-type structure as a representative of $(R_{1.5}Mg_{0.5})Ni_7$ compounds can absorb and desorb hydrogen under moderate conditions [30]. Its hydride formation enthalpy is about −31.4 kJ/mol H_2, which is close to −30 kJ/mol H_2 for the $LaNi_5$−H_2 system [34]. However, hydrogen storage properties of $(La_{1.66}Mg_{0.34})Ni_7$ have not been reported to date. Moreover, the effects of partial substitution for La and Ni in the $(La_{1.66}Mg_{0.34})Ni_7$ compound on the thermodynamics of hydrogen absorption and desorption also interest us because alloying is an effective method to improve hydrogen storage properties. Hence, the hydrogen absorption-desorption properties of $(La_{1.66}Mg_{0.34})Ni_7$-based compounds were finally investigated.

2. EXPERIMENTAL DETAILS

2.1 Sample Preparation

$(La_{1.66}Mg_{0.34})Ni_7$ and ($(La_{1.26}R_{0.4}Mg_{0.34})(Ni_{6.2}Co_{0.6}Al_{0.2})$ R=La, Ce, Pr, Nd, Y, Sm, Gd) were prepared by induction melting approach at 0.4 MPa of Ar. atmosphere. The ingots were wrapped in a thallium (Ta) foil, sealed in stainless steel tubes under Ar pressure (0.1 MPa) and annealed for a week at 1173K. Due to the high vapor pressure of Mg element, 10 wt.% excess of Mg element was necessary during melting. The purity of all elements was above 99 wt.%.

2.2 Structural Characterization

The annealed alloys were crushed mechanically into powder (<38μm) for x-ray diffraction(XRD) measurements and powder from 54μm to 61μm for electrode test. XRD measurements were performed on a Rigaku D/max-2400 diffractometer with Cu radiation and a power of 40 kV × 150 mA. The patterns were recorded over the range from 15° to 90°in 2θ by step of 0.02°. Then the collected data were analyzed by the Rietveld method [35] using Fullprof 2K software [36] to get the lattice parameters and phase abundance.

The microscopic structure and the composition for annealed alloys were examined by Electron probe microanalyzer (EPMA-1600). After hydrogenation, the samples were examined using a transmission electron microscope (TEM, JEOL, JEM-2010, Japan) and a scanning electron microscope (SEM, JEOL, JSM-6701F, Japan) at an accelerating voltage of 8 kV.

2.3 Hydrogen Absorption and Desorption

To investigate the hydrogen storage properties of $(La_{1.66}Mg_{0.34})Ni_7$-based compounds, pressure-composition (P−C) isotherms were measured using a Sieverts-type apparatus (Beijing Nonferrous Metal Research Institute, China) at 298 K. Prior to formal measurements, powder samples were heated in a vacuum at 373 K for 2 h and then activated by repeatedly hydriding−dehydriding at 333 K three times.

3. RESULTS AND DISCUSSION

3.1 Alloy crystal structure

Fig.1 shows the XRD patterns for $(La_{1.66}Mg_{0.34})Ni_7$ and $La_{0.63}R_{0.2}Mg_{0.17}Ni_{3.1}Co_{0.3}Al_{0.1}$ (R=La, Ce, Pr, Nd, Y, Sm, Gd) alloys. Fig.2 shows the Rietveld refinement patterns of $(La_{1.66}Mg_{0.34})Ni_7$ and $La_{0.63}R_{0.2}Mg_{0.17}Ni_{3.1}Co_{0.3}Al_{0.1}$ (R = La, Gd) alloy, respectively. Structure characteristics of different R-substituted alloys are tabulated in Table 1. Based on the XRD data, the crystal structure of $(La, Mg)_2Ni_7$ seems to retain the hexagonal Ce_2Ni_7-structure type. The back scattered electron (BSE) image of $La_{0.63}R_{0.2}Mg_{0.17}Ni_{3.1}Co_{0.3}Al_{0.1}$ (R=La, Pr, Y, Gd) and are shown in Fig 3. A light grey area (α) and black area (β) can be seen in Fig 3 ((a) - (d)). The WDS analyses in Fig 3 show that the light grey (α) and black area (β) correspond to A_2B_7- and AB_5-type phase, respectively. The results are consistent with those obtained from XRD.

The crystallographic parameters of Ce_2Ni_7 unit cell for the alloy of $(La_{1.66}Mg_{0.34})Ni_7$ are tabulated in Table 2, according to Rietveld analysis. The Rietveld refinements show that Mg partly substitutes La, exclusively in the $LaNi_2$ slabs (4f site) and occupies statistically ~35% of the available sites. The well crystalline phase reveals close similarity to La_2Ni_7 but with reduced unit cell parameters due to the smaller magnesium and rare earth radii (see Table3). Compared to pure La_2Ni_7, the contraction of the unit cell due to the introduced Mg for$(La_{1.66}Mg_{0.34})Ni_7$ is: $\triangle V/V = -1.6\%$ with $\triangle a/a$

= -0.2% and $\triangle c/c$ = -1.3%, without any change of the symmetry (hexagonal, P6$_3$/mmc). For La$_{0.83}$Mg$_{0.17}$Ni$_{3.1}$Co$_{0.3}$Al$_{0.1}$ and La$_{0.63}$- Gd$_{0.2}$Mg$_{0.17}$Ni$_{3.1}$Co$_{0.3}$Al$_{0.1}$, the contraction of the Ce$_2$Ni$_7$ (hexagonal, P6$_3$/mmc) unit cell is: $\triangle V/V$ = -0.97% with $\triangle c/c$ = -1.1%, $\triangle V/V$ = -2.2% with $\triangle a/a$ =-0.4% and $\triangle c/c$ = -1.5%, respectively. Because of the large difference in the atomic radii (La (1.877 Å) and Mg (1.602 Å), Ni (1.24 Å) Co (1.26 Å) and Al (1.43 Å)) and selective occupation of Mg in the 4f sites, Co and Al in the Ni sites, the main contraction proceed in the AB$_2$ layers. These results are in agreement with published ones [20, 32, 37, 38]. So we hypothesize that R only occupies the 4f sites and improves the contraction in the AB$_2$ slabs, this is one of the reason why La$_{0.63}$R$_{0.2}$Mg$_{0.17}$Ni$_{3.1}$Co$_{0.3}$Al$_{0.1}$ (R = Pr, Nd, Sm, Gd, Y) exhibits good electrochemical properties [32].

Table 1. Characteristics of phases for (La$_{1.66}$Mg$_{0.34}$)Ni$_7$ and La$_{0.63}$R$_{0.2}$Mg$_{0.17}$Ni$_{3.1}$Co$_{0.3}$Al$_{0.1}$ alloys.

Sample	Phase	Space Group	Lattice constants (Å)				Phase abundance (wt.%)
			a	c	V	c/a	
(La$_{1.66}$Mg$_{0.34}$)Ni$_7$	(La,Mg)$_2$(Ni,Co)$_7$	R-3m	5.051	36.399	804.284	7.206	4.74
	(La,Mg)$_2$(Ni,Co)$_7$	P6$_3$/mmc	5.050	24.389	538.699	4.830	95.17
	La(Ni,Co)$_5$	P6/mmm	5.045	3.980	87.74	0.789	0.09
R = La	(La,Mg)$_2$(Ni,Co)$_7$	R-3m	5.098	36.662	825.227	7.191	3.61
	(La,Mg)$_2$(Ni,Co)$_7$	P6$_3$/mmc	5.061	24.438	542.148	4.829	95.23
	La(Ni,Co)$_5$	P6/mmm	5.018	4.034	87.964	0.804	1.16
R = Ce	(La,Mg)$_2$(Ni,Co)$_7$	R-3m	4.949	36.470	773.608	7.369	3.74
	(La,Mg)$_2$(Ni,Co)$_7$	P6$_3$/mmc	5.032	24.399	535.040	4.849	95.11
	La(Ni,Co)$_5$	P6/mmm	5.056	4.063	89.954	0.804	1.16
R = Pr	(La,Mg)$_2$(Ni,Co)$_7$	R-3m	5.338	37.945	936.514	7.108	1.73
	(La,Mg)$_2$(Ni,Co)$_7$	P6$_3$/mmc	5.049	24.401	538.616	4.833	71.84
	La(Ni,Co)$_5$	P6/mmm	5.019	3.996	87.163	0.796	26.43
R = Nd	(La,Mg)$_2$(Ni,Co)$_7$	R-3m	5.037	35.689	784.152	7.085	6.21
	(La,Mg)$_2$(Ni,Co)$_7$	P6$_3$/mmc	5.048	24.392	538.268	4.832	86.10
	La(Ni,Co)$_5$	P6/mmm	5.019	3.998	87.195	0.797	7.69
R = Y	(La,Mg)$_2$(Ni,Co)$_7$	R-3m	5.031	36.469	799.431	7.249	1.08
	(La,Mg)$_2$(Ni,Co)$_7$	P6$_3$/mmc	5.029	24.302	532.299	4.832	98.7
	La(Ni,Co)$_5$	P6/mmm	5.016	4.013	87.444	0.800	0.22
R = Sm	(La,Mg)$_2$(Ni,Co)$_7$	R-3m	4.784	36.336	720.141	7.595	9.45
	(La,Mg)$_2$(Ni,Co)$_7$	P6$_3$/mmc	5.043	24.361	536.434	4.831	90.54
	La(Ni,Co)$_5$	P6/mmm	5.035	4.030	88.486	0.800	0.00
R = Gd	(La,Mg)$_2$(Ni,Co)$_7$	R-3m	5.079	36.541	816.295	7.195	2.40
	(La,Mg)$_2$(Ni,Co)$_7$	P6$_3$/mmc	5.039	24.351	535.507	4.833	94.16
	La(Ni,Co)$_5$	P6/mmm	4.995	4.089	88.359	0.819	3.44

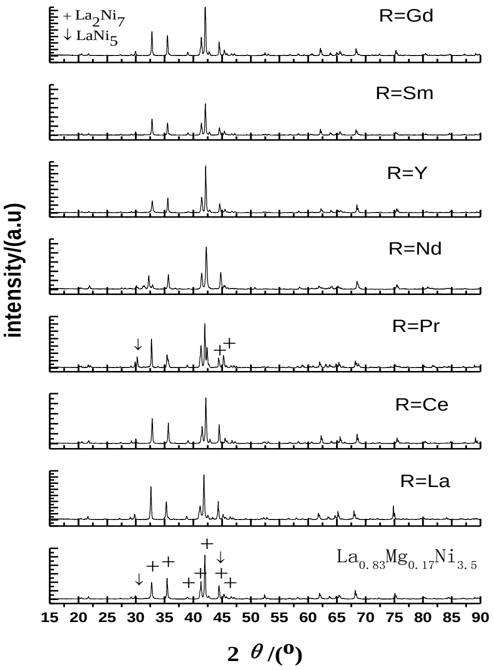

Figure 1. XRD patterns for $(La_{1.66}Mg_{0.34})Ni_7$ and $La_{0.63}R_{0.2}Mg_{0.17}Ni_{3.1}Co_{0.3}Al_{0.1}$ alloys.

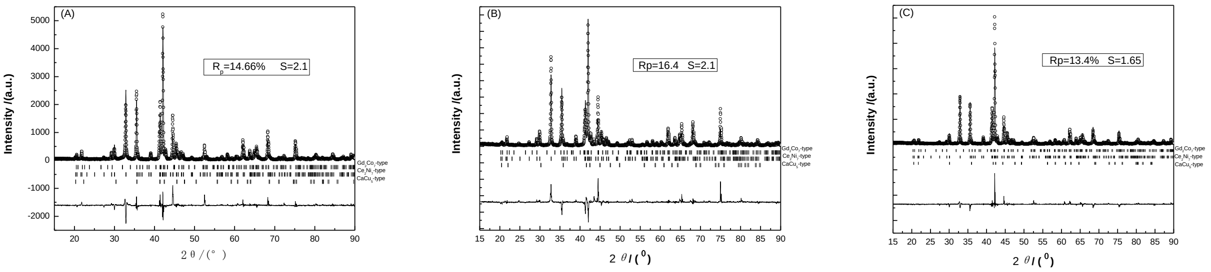

Figure 2. Rietveld refinement patterns for $(La_{1.66}Mg_{0.34})Ni_7$ and $La_{0.63}R_{0.2}Mg_{0.17}Ni_{3.1}Co_{0.3}Al_{0.1}$ alloy: (A) $(La_{1.66}Mg_{0.34})Ni_7$ (B) R = La, (C) R = Gd.

Table 2. Crystallographic parameters of $(La_{1.66}Mg_{0.34})Ni_7$ alloy with space group $P6_3/mmc$.

Atom	Symmetry	x	y	z	B_{iso}	Occupancy
La 1	4f	1/3	2/3	0.02698(8)	1.03(6)	0.66(1)
La 2	4f	1/3	2/3	0.17108(6)	0.98(4)	1.00(1)
Mg 1	4f	1/3	2/3	0.02698(8)	1.03(-)	0.35(-)
Ni 1	2a	0	0	0	0.9(1)	1.00(-)
Ni 2	4e	0	0	0.1678(1)	0.98(7)	1.00(-)
Ni 3	4f	1/3	2/3	0.8329(1)	0.61(6)	1.00(-)
Ni 4	6h	0.8326(8)	0.665(2)	1/4	0.50(6)	1.00(-)
Ni 5	12k	0.8330(5)	0.666(1)	0.08486(6)	0.84(4)	1.00(-)

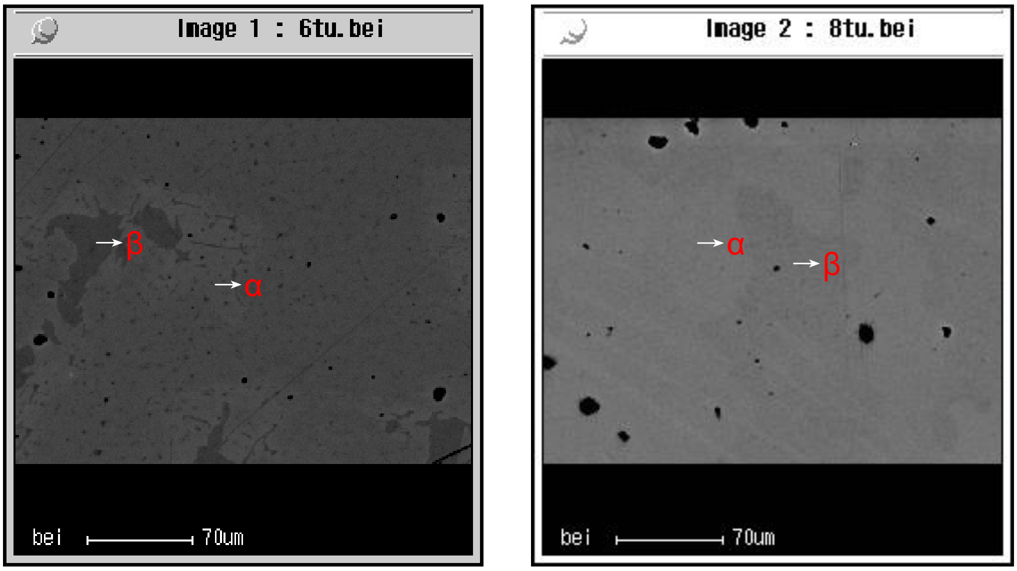

(a) R = La (b) R = Pr

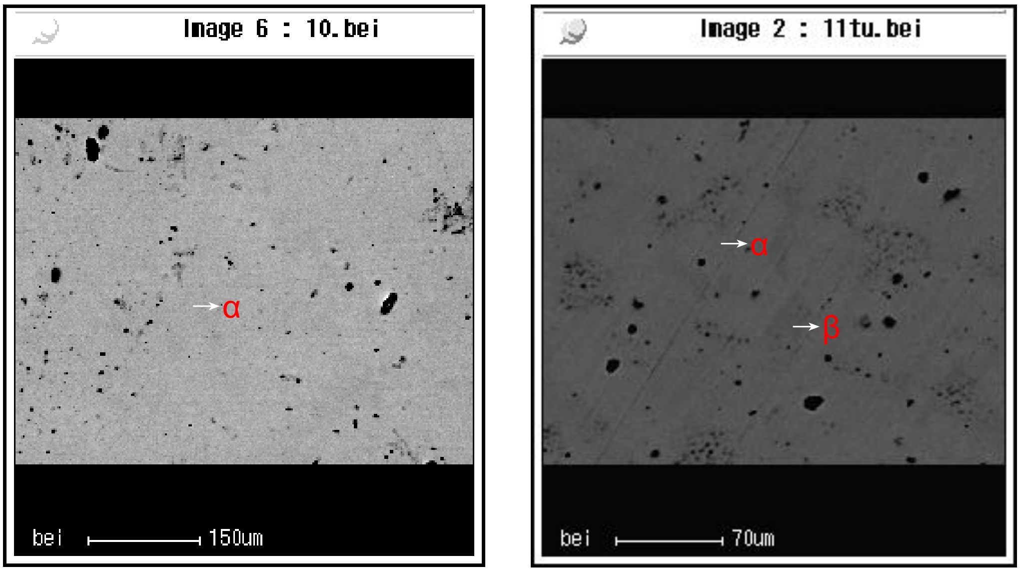

(c) R = Y (d) R = Gd

Figure 3. Back scattered electron images for $La_{0.63}R_{0.2}Mg_{0.17}Ni_{3.1}Co_{0.3}Al_{0.1}$ alloys (a) R = La (b) R = Pr (c) R = Y (d) R = Gd.

Table 3. Comparison of selected crystallographic parameters for chosen hexagonal Ce_2Ni_7-type compounds in La-Ni, La-Mg-Ni and La-R-Mg-Ni systems.

Parameters	Compound				
	La_2Ni_7 [29]	$La_{1.5}Mg_{0.5}Ni_7$ [30]	$La_{1.66}Mg_{0.34}Ni_7$	$La_{0.83}Mg_{0.17}Ni_{3.1}Co_{0.3}Al_{0.1}$	$La_{0.83}Gd_{0.2}Mg_{0.17}Ni_{3.1}Co_{0.3}Al_{0.1}$
a (Å)	5.058	5.0285	5.050	5.061	5.039
c (Å)	24.71	24.222	24.389	24.438	24.351
V (Å^3)	547.47	530.42	538.699	542.148	535.507
V_{AB5} (Å^3)	177.37	175.77	-	-	-
V_{AB2} (Å^3)	96.35	89.01	-	-	-
Δa/a (%)	-	-0.6	-0.2	0.06	-0.4
Δc/c (%)	-	-2.0	-1.3	-1.1	-1.5
ΔV/V (%)	-	-3.1	-1.6	-0.97	-2.2

3.2 Thermodynamic (P-C isotherm) measurements

The single plateau behaviour is clearly seen in the absorption and desorption isotherms at 298K (Fig. 4). It can be seen that the absorption-desorption plateau became flatter and 298K (Fig. 4). It can be seen that the absorption-desorption plateau became flatter and isotherms are not horizontal, it is obvious that the plateau slope gradually decrease from $(La_{1.66}Mg_{0.34})Ni_7$ to Gd-substituted alloy. Similar observations have been made by Oesterreicher et al. [39], who noticed that $La_2Ni_7H_{10}$ decomposes with hydrogen desorption. Such disproportionation also made impossible measurements of the thermodynamic data for the chemically related $LaNi_3$-H and $LaNi_2$-H systems, where hydrides easily become amorphous and, later, disproportionate. This can be further confirmed by the result of TEM image shown in Fig. 5. Fig. 5(A) and (B) show TEM images of $La_{1.66}Mg_{0.34}Ni_7H_{6.4}$ and $La_{0.63}Gd_{0.2}Mg_{0.17}Ni_{3.1}Co_{0.3}Al_{0.1}H_{8.8}$, respectively. Both of them exhibit amorphous phenomenon, but the amorphous effect of $La_{0.63}Gd_{0.2}Mg_{0.17}Ni_{3.1}Co_{0.3}Al_{0.1}$ alloy is more slight.

In addition, the hydrogen content also gradually increased from 0.98 wt.% to 1.353 wt.%. In our work, the maximum hydrogen capacity at 298K is slightly lower than for $La_{1.5}Mg_{0.5}Ni_7$ at 298K [30].

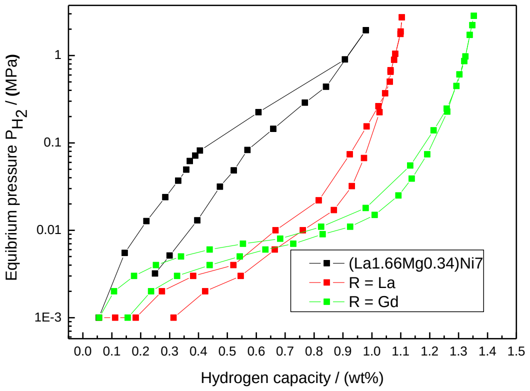

Figure 4. P-C isotherms of $(La_{1.66}Mg_{0.34})Ni_7$ and $La_{0.63}R_{0.2}Mg_{0.17}Ni_{3.1}Co_{0.3}Al_{0.1}$ (R = La, Gd) alloys at 298K.

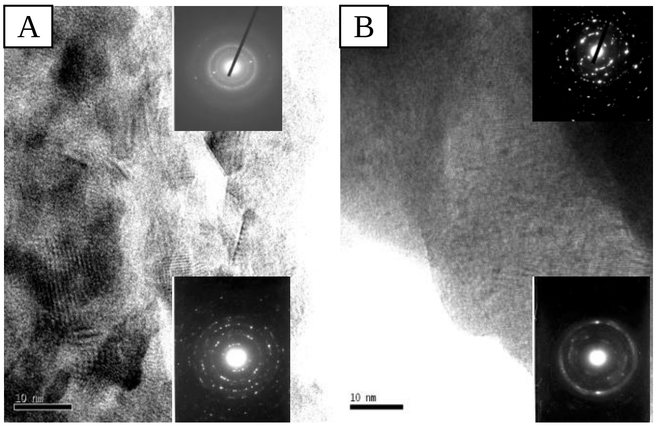

Figure 5. TEM image of $La_{1.66}Mg_{0.34}Ni_7H_{6.4}$ and $La_{0.63}Gd_{0.2}Mg_{0.17}Ni_{3.1}Co_{0.3}Al_{0.1}H_{4.4}$ hydrides.

3.3 *Study of the hydride*

The hydrogenation of the $(La_{1.66}Mg_{0.34})Ni_7$ and $La_{0.63}R_{0.2}Mg_{0.17}Ni_{3.1}Co_{0.3}Al_{0.1}$ (R = La, Gd) alloy resulted in the formation of the hydride with the composition of $La_{1.66}Mg_{0.34}Ni_7H_{6.4}$, $La_{0.83}Mg_{0.17}Ni_{3.1}Co_{0.3}Al_{0.1}H_{3.55}$, and $La_{0.63}Gd_{0.2}Mg_{0.17}Ni_{3.1}Co_{0.3}Al_{0.1}H_{4.4}$, as follows from the PCT isotherm at 298K (Fig. 4). The hydrogenation is accompanied by isotropic expansion of the $La_{1.66}Mg_{0.34}Ni_7H_{6.4}$ unit cell, $\triangle a/a = 7.3\%$ and $\triangle c/c = 9.1\%$. These values are close to those observed for the formation of the $La_{1.5}Mg_{0.5}Ni_7H_{9.3}$ of the filled Ce_2Ni_7 type of structure [30] and are in sharp contrast with the values for the hydride of the isostructural non-substituted La_2Ni_7 alloy, which expands anisotropically [29] (see Table 4). The isotropic expansion of the unit cell of $La_{1.66}Mg_{0.34}Ni_7$ indicates that the hydrogenation leads to an even distribution of hydrogen through all the slabs of the structure, similarly as it has been observed for $La_{1.5}Mg_{0.5}Ni_7$ [30]. This is in contrast to anisotropic hydrides, where only Laves phase-type slabs accommodate hydrogen, leaving the $CaCu_5$-type layers unexpanded. However, when Ni is partially replaced by Co and Al, the hydrogenation is accompanied by anisotropic expansion in $La_{0.83}Mg_{0.17}Ni_{3.1}Co_{0.3}Al_{0.1}$ unit cell: $\triangle a/a = 3.6\%$ and $\triangle c/c = -3.5\%$. For $La_{0.63}Gd_{0.2}Mg_{0.17}Ni_{3.1}Co_{0.3}Al_{0.1}$ unit cell, the hydrogenation is accompanied by slight isotropic contraction, $\triangle a/a = -0.2\%$ and $\triangle c/c = -0.8\%$. This value is very close to the isostructural non-substituted La_2Ni_7 alloy. So $La_{0.63}R_{0.2}Mg_{0.17}Ni_{3.1}Co_{0.3}Al_{0.1}H_X$ is in contrast to other hydrides, where the expansion of unit cell is large after hydrogenation.

Fig.6 (A) and (B) shows the XRD patterns for hydrides and the Rietveld refinement patterns of $La_{0.63}Gd_{0.2}Mg_{0.17}Ni_{3.1}Co_{0.3}Al_{0.1}H_{4.4}$, respectively. SEM are employed to investigate the surface morphology of the $La_{1.66}Mg_{0.34}Ni_7H_{6.4}$, $La_{0.83}Mg_{0.17}Ni_{3.1}Co_{0.3}Al_{0.1}H_{3.55}$, and $La_{0.63}Gd_{0.2}Mg_{0.17}Ni_{3.1}Co_{0.3}Al_{0.1}H_{4.4}$. Fig. 7 (A) – (C) show the SEM images of above three hydrides, respectively. Average particle size is in the order: $La_{1.66}Mg_{0.34}Ni_7H_{6.4} < La_{0.83}Mg_{0.17}Ni_{3.1}Co_{0.3}Al_{0.1}H_{3.55} < La_{0.63}Gd_{0.2}Mg_{0.17}Ni_{3.1}Co_{0.3}Al_{0.1}H_{4.4}$. The results are consistent with those obtained from unit cell volume ($\triangle V/V$).

Table 4. Comparison of selected crystallographic parameters for chosen hexagonal Ce_2Ni_7-type hydrides in La-Ni, La-Mg-Ni and La-R-Mg-Ni systems.

Parameters	Compound					
	La_2Ni_7 [29]	$La_2Ni_7D_{6.5}$ [29]	$La_{1.5}Mg_{0.5}Ni_7H_{9.3}$ [30]	$La_{1.66}Mg_{0.34}Ni_7H_{6.4}$	$La_{0.83}Mg_{0.17}Ni_{3.1}Co_{0.3}Al_{0.1}H_{3.55}$	$La_{0.83}Gd_{0.2}Mg_{0.17}Ni_{3.1}Co_{0.3}Al_{0.1}H_{4.4}$
a (Å)	5.058	4.9534	5.4121	5.4151	5.2388	5.0457
c (Å)	24.71	29.579	26.589	26.5392	23.8522	24.5070
V (Å^3)	547.47	628.52	674.48	673.95	566.917	540.325
V_{AB5} (Å^3)	177.37	171.96	-	-	-	-
V_{AB2} (Å^3)	96.35	142.30	-	-	-	-
$\Delta a/a$ (%)	-	-2.1	7.63	7.3	3.6	-0.2
$\Delta c/c$ (%)	-	19.7	9.77	9.1	-3.5	-0.8
$\Delta V/V$ (%)	-	14.8	25.2	25.6	3.6	-1.3

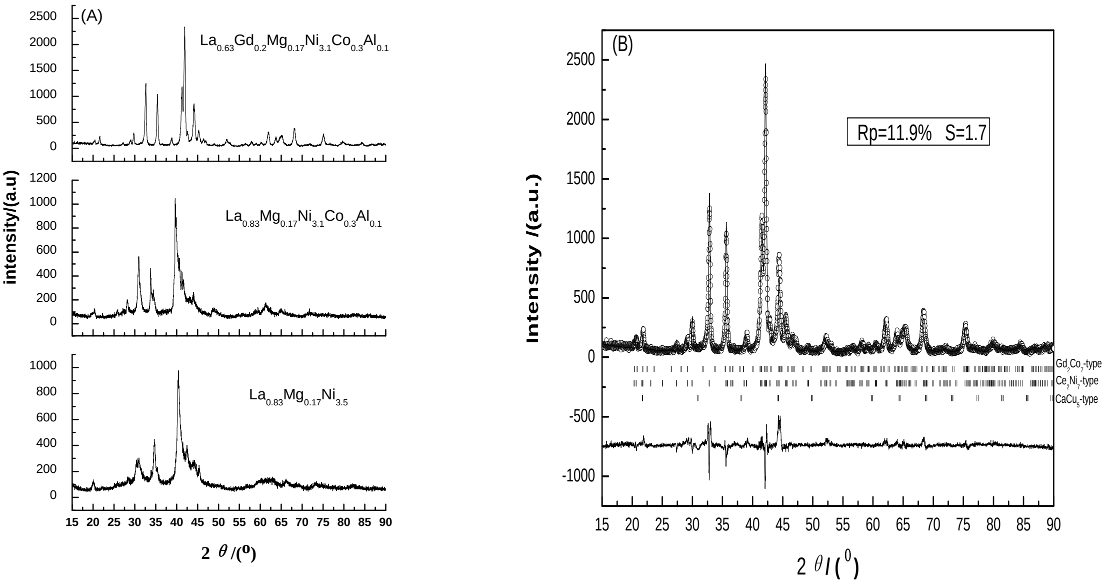

Figure 6. XRD patterns for $(La_{1.66}Mg_{0.34})Ni_7$ and $La_{0.63}R_{0.2}Mg_{0.17}Ni_{3.1}Co_{0.3}Al_{0.1}$ (R = La, Gd) hydrides (A) and rietveld refinement patterns for $La_{0.63}Gd_{0.2}Mg_{0.17}Ni_{3.1}Co_{0.3}Al_{0.1}$ hydrides (B).

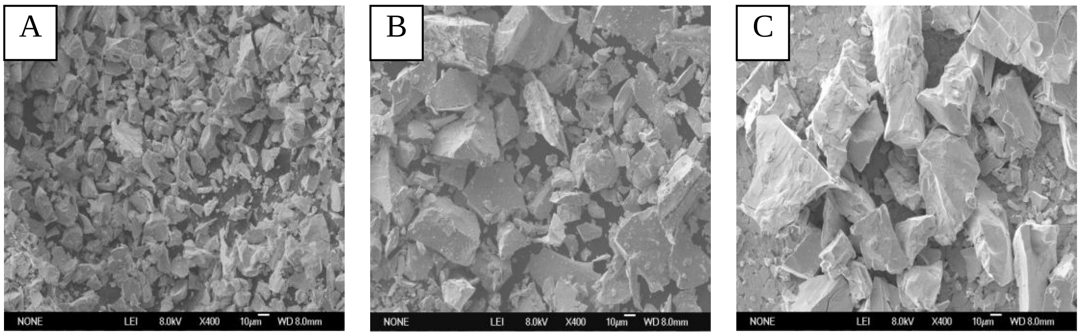

Figure 7. SEM image of $(La_{1.66}Mg_{0.34})Ni_7$ (A) and $La_{0.63}R_{0.2}Mg_{0.17}Ni_{3.1}Co_{0.3}Al_{0.1}$ hydrides: R = La(B), R = Gd (C).

4. CONCLUSIONS

A systematic investigation of the structural and hydrogen storage properties of $(La_{1.66}Mg_{0.34})Ni_7$-based compounds was conducted in the this study. Some conclusion can be summarized:

1) The $(La_{1.66}Mg_{0.34})Ni_7$-based alloy is composed of a hexagonal phase (Ce_2Ni_7) and accompanied by minor impurity phases $LaNi_5$, 3R-Gd_2Co_7.

2) These changes are caused by partial replacement of La by R and include:

(a) Increase of the reversible hydrogen storage capacity;

(b) Absence of amorphous phenomenon and disproportionation of the metal matrix on cycling of hydrogenation and decomposition because of the stabilisation of the metal sublattice by R;

(c) Change of the mechanism of hydrogenation from an “anisotropic” hydride to an“isotropic” one;

(d) Little change of the unit cell parameters between $La_{0.63}R_{0.2}Mg_{0.17}Ni_{3.1}Co_{0.3}Al_{0.1}H_x$ and non-substituted La_2Ni_7 alloy.

The present work contributes to the design of new low-Mg R-Mg-Ni materials with higher hydrogen discharge capacities for technological applications such as electrode materials in rechargeable Ni/MH batteries.

ACKNOWLEDGEMENTS
This work was supported by the National Nature Science Foundation of China (No. 50941019), the Nature Science Foundation of Shandong Province (No. ZR2014EMP012), the Nature Science Foundation of Shandong Province (No. ZR2015PB007) and the Science and Technology Development Plan of Bingzhou (No. 2014ZC0216).

References

1. A. C. Dillon, K. M. Jones, T. A. Bekkedahl, C. H. Kiang, D. S. Bethune, M. J. Heben, *Nature*, 386 (1997) 377.
2. J. J. Liu, S. M. Han, D. Han, Y. Li, S. Q. Yang, L. Zhang, Y. M. Zhao, *J. Power Sources*, 287 (2015) 237.
3. R. F. Li, R. H. Yu, X. F. Liu, J. Wan, F. Wang, *Electrochim. Acta*, 158 (2015) 89.
4. Dymek, Martyna, Rozdzynska-Kielbik, Beata, Paviyuk, Volodymyr V., Henryk Bala, *J. Alloys Compd.*, 644 (2015) 916.
5. S. C. Li, B. Q. Wen, X. Li, J. Zhai, *J. Alloys Compd.*, 654 (2016) 580.
6. K. Young, T. Ouchi, J. Nei, L. Wang, *J. Alloys Compd.*, 654 (2016) 216.
7. X. G. Shang, S. Lu, X. Y. Peng, Y. P. Fan, B. Q. Zhang, Z. Zhang, B. Z. Liu, *Int. J Electrochem. Sci.*, 9 (2014) 4913.
8. Y. M. Li, H. P. Ren, Y. H. Zhang, Z. C. Liu, H. W. Zhang, *Int. J Hydrogen Energy*, 40 (2015) 7093.
9. K.Kadir, T.Sakai, I.Uehara, *J. Alloys Compd.*, 257 (1997) 115.
10. K. Kadir, T. Sakai, I. Uehara, *J. Alloys Compd.*, 302 (2000) 112.
11. T. Kohno, H. Yoshida, F. Kawashima, T. Inaba, I. Sakai, M. Yamamoto, M. Kanda, *J. Alloys Compd.*, 311 (2000) L5.
12. Y. C. Wang, Y. Li, W. Z. Shen, Y. R. Peng, Jerry Y. H. Che, S. Q. Yang, S. M. Han, *J. Solid. State Electrochem.*, 19 (2015) 1419.
13. K. Iwase, K. Sakaki, Y. Nakamura, E. Akiba, *Inorg. Chem.*, 49 (2010) 8763.
14. Y. Chai, K. Asano, K. Sakaki, H. Enoki, E. Akiba, *J. Alloys Compd.*, 485 (2009) 174.
15. R. F. Li, P. Z. Xu, Y. M. Zhao, J. Wang, X. F. Liu, R. H. Yu, *J. Power Sources*, 270 (2014) 21.
16. A. Ferey, F. Cuevas, M. Latroche, B. Knosp, P. Bernard, *Electrochim. Acta*, 54 (2009) 1710.
17. B. P. Wang, L. M. Zhao, C. S. Cai, S. X. Wang, *Int. J Hydrogen Energy*, 39 (2014) 10374.
18. J. Nakamura, K. Iwase, H. Hayakawa, Y. Nakamura, E. Akiba, *J. Phys. Chem. C*, 113 (2009) 5853.
19. Y. Nakamura, J. Nakamura, K. Iwase, E. Akiba, *Nucl. Instrum. Meth. A*, 600 (2009) 297.
20. T. Ozaki, M. Kanemoto, T. Kakeya, Y. Kitano, M. Kuzuhara, M. Watada, S. Tanase, T. Sakai, *J. Alloys Compd.*, 446 (2007) 620.
21. Q.A. Zhang, M.H. Fang, T.Z. Si, F. Fang, D. L. Sun, L.Z. Ouyang, M. Zhu, *J. Phys. Chem. C*, 114 (2010) 11686.
22. K. L. Lim, Y. N. Liu, Q. A. Zhang, S. L. L. Chan, *Int. J Hydrogen Energy*, 39 (2014) 10537.
23. X. Tian, G. H. Yun, H. Y. Wang, T. Shang, Z. Q. Yao, W. Wei, X. X. Liang, *Int. J Hydrogen Energy*, 39 (2014) 8474.
24. F.L. Zhang, Y.C. Luo, D.H. Wang, R.X. Yan, L. Kang, J.H. Chen, *J. Alloys Compd.*, 439 (2007)

181.
25. W. Zhu, C. Tan, J. B. Xu, Z. X. Li, *J. Electrochem. Soc.*, 161 (2014) A89.
26. R.V. Denys, V.A. Yartys, M. Sato, A.B. Riabov, R.G. Delaplane, *J. Solid. State Chem.*, 180 (2007) 2566.
27. Y.E. Filinchuk, K. Yvon, H. Emerich, *Inorg. Chem.*, 46 (2007) 2914.
28. R.V. Denys, A.B. Riabov, R. Černý, I.V. Koval'chuk, I.Yu. Zavaliy, *J. Solid. State Chem.*, 187 (2012) 1.
29. V.A. Yartys, A.B. Riabov, R.V. Denys, M. Sato, R.G. Delaplane, *J. Alloys Compd.*, 408 (2010) 273.
30. R.V. Denys, A.B. Riabov, V.A. Yartys, M. Sato, R.G. Delaplane, *J. Solid. State Chem.*, 181 (2008) 812.
31. M.N. Guzik, B.C. Hauback, K. Yvon, *J. Solid. State Chem.*, 186 (2012) 9.
32. Z.J. Gao, Y.C. Luo, L. Kang, *New J. Chem.*, 37 (2013) 1105.
33. K.H.J. Buschow, A.S. Van Der Goot, *J. Less-Comm. Mat.*, 22 (1970) 419.
34. J. H. N. van Vucht, F. A. Kuijpers, H. C. A. M. Bruning, *Philips. Res. Rep.*, 25 (1970) 133.
35. R. A. Young, *The Rietveld Method, Introduction to the Rietveld Method*; R. A. Roung Eds.; Oxford University Press Inc; New York, 1995, p.1.
36. Z.J. Gao, Y.C. Luo, R. F. Li, Z. Lin, L. Kang, *J. Power Sources*, 241 (2013) 509.
37. W. K. Du, S. B. Cao, Y. Li, L. Zhang, Y. M. Zhao, S. Q. Yang, S. M. Han, *J. Electrochem. Soc.*, 162 (2015) A2180.
38. L. Zhang, S. B. Cao, Y. Li, Y. M. Zhao, W. K. Du, Y. Q. Ding, S. M. Han, *J. Electrochem. Soc.*, 162 (2015) A2218.
39. H. Oesterreicher, J. Clinton, H. Bittner, *Mater. Res. Bull.*, 11 (1976) 1241.